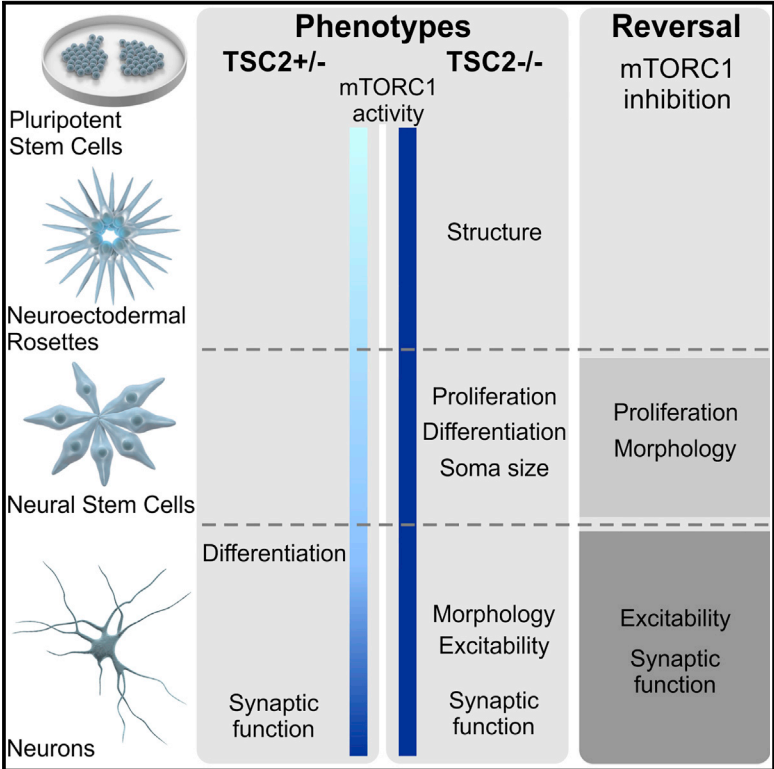# mTORC1 Inhibition Corrects Neurodevelopmental and Synaptic Alterations in a Human Stem Cell Model of Tuberous Sclerosis

Graphical Abstract

Authors

Veronica Costa, Stefan Aigner, Mirko Vukcevic, ..., Anirvan Ghosh, Josef Bischofberger, Ravi Jagasia

Correspondence

veronica.costa@roche.com (V.C.),
ravi.jagasia@roche.com (R.J.)

In Brief

The neurodevelopmental disorder tuberous sclerosis is caused by loss of *TSC1/2*, negative regulators of mTORC1. Combining genome editing technology and human stem cell differentiation, Costa et al. characterize stage-specific molecular, cellular, and synaptic alterations in neurons with *TSC2* deletion and show that mTORC1 inhibition corrects defects in synaptic function independently of early neurodevelopmental abnormalities.

Highlights

- *TSC2* deletion causes gene-dosage-dependent mTORC1 hyperactivity in neurodevelopment

- *TSC2* deletion causes alterations in pathways and genes associated with autism

- $TSC2^{+/-}$ and $TSC2^{-/-}$ human neurons show stage-specific cellular and synaptic defects

- mTORC1 inhibition corrects synaptic defects independently of early neurodevelopment

mTORC1 Inhibition Corrects Neurodevelopmental and Synaptic Alterations in a Human Stem Cell Model of Tuberous Sclerosis

Veronica Costa,[1,8,*] Stefan Aigner,[1,8,9] Mirko Vukcevic,[5,8] Evelyn Sauter,[1,10] Katharina Behr,[5] Martin Ebeling,[2] Tom Dunkley,[2] Arno Friedlein,[2] Sannah Zoffmann,[3] Claas A. Meyer,[3] Frédéric Knoflach,[1] Sebastian Lugert,[1] Christoph Patsch,[3] Fatiha Fjeldskaar,[1] Laurie Chicha-Gaudimier,[4] Anna Kiialainen,[2] Paolo Piraino,[6] Marc Bedoucha,[1] Martin Graf,[3] Sebastian Jessberger,[7] Anirvan Ghosh,[1] Josef Bischofberger,[5] and Ravi Jagasia[1,*]

[1]Roche Pharmaceutical Research and Early Development, Neuroscience Ophthalmology and Rare Diseases Discovery & Translational Area, Roche Innovation Center Basel, F. Hoffmann-La Roche Ltd., Grenzacherstrasse 124, 4070 Basel, Switzerland
[2]Roche Pharmaceutical Research and Early Development, Pharmaceutical Sciences, Roche Innovation Center Basel, F. Hoffmann-La Roche Ltd., Grenzacherstrasse 124, 4070 Basel, Switzerland
[3]Roche Pharmaceutical Research and Early Development, Therapeutic Modalities, Roche Innovation Center Basel, F. Hoffmann-La Roche Ltd., Grenzacherstrasse 124, 4070 Basel, Switzerland
[4]Department of Neurosurgery, Universitätsspital Basel, ZLF 20 Hebelstrasse, 4031 Basel, Switzerland
[5]Department of Biomedicine, University of Basel, Pestalozzistrasse 20, 4056 Basel, Switzerland
[6]Pvalue Research SRL, 29015 Castel San Giovanni, Italy
[7]Brain Research Institute, Faculty of Medicine and Science, University of Zurich, 8057 Zurich, Switzerland
[8]Co-first author
[9]Present address: Department of Cellular and Molecular Medicine, School of Medicine, University of California, San Diego, La Jolla, CA 92093, USA
[10]Present address: Center for Regenerative Therapies Dresden, Technische Universität Dresden, 01307 Dresden, Germany
*Correspondence: veronica.costa@roche.com (V.C.), ravi.jagasia@roche.com (R.J.)
http://dx.doi.org/10.1016/j.celrep.2016.02.090

SUMMARY

Hyperfunction of the mTORC1 pathway has been associated with idiopathic and syndromic forms of autism spectrum disorder (ASD), including tuberous sclerosis, caused by loss of either *TSC1* or *TSC2*. It remains largely unknown how developmental processes and biochemical signaling affected by mTORC1 dysregulation contribute to human neuronal dysfunction. Here, we have characterized multiple stages of neurogenesis and synapse formation in human neurons derived from *TSC2*-deleted pluripotent stem cells. Homozygous *TSC2* deletion causes severe developmental abnormalities that recapitulate pathological hallmarks of cortical malformations in patients. Both *TSC2*$^{+/-}$ and *TSC2*$^{-/-}$ neurons display altered synaptic transmission paralleled by molecular changes in pathways associated with autism, suggesting the convergence of pathological mechanisms in ASD. Pharmacological inhibition of mTORC1 corrects developmental abnormalities and synaptic dysfunction during independent developmental stages. Our results uncouple stage-specific roles of mTORC1 in human neuronal development and contribute to a better understanding of the onset of neuronal pathophysiology in tuberous sclerosis.

INTRODUCTION

Increased activity of the mammalian target of rapamycin complex 1 (mTORC1) pathway has been implicated in autism spectrum disorder (ASD) and related neurodevelopmental disorders. Indeed, several monogenic disorders associated with a high rate of autism are caused by mutations in negative regulators of the pathway (Bourgeron, 2009), and mTORC1 overactivation has been detected in temporal lobe of patients with idiopathic ASD (Tang et al., 2014). Moreover, alterations in processes downstream of mTORC1 recapitulate ASD-like behavioral abnormalities and cellular pathology in mice (Santini et al., 2013; Gkogkas et al., 2013; Tang et al., 2014). Thus, a better understanding of the molecular and cellular consequences of mTORC1 hyperfunction might help to identify novel targets for therapeutic intervention.

Tuberous sclerosis (TSC) is a severe multisystem disorder that presents with complex neuropsychiatric symptoms including autism, intellectual disability, and epilepsy (Crino et al., 2006; Rosser et al., 2006). Neuroanatomical abnormalities include formation of cortical tubers, which are disorganized regions of the cortex characterized by the presence of dysplastic neurons with immature electrophysiological properties (Cepeda et al., 2012). The disease is caused by heterozygous loss-of-function mutations in the genes coding for TSC1 or TSC2. Loss of heterozygosity due to somatic mutations of the functional allele has been detected in hamartomas, while its role in tuber formation remains controversial (Henske et al., 1997; Chan et al., 2004; Crino et al., 2010; Qin et al., 2010). TSC1 and TSC2 form a

heterodimeric complex that functions as a negative regulator of mTORC1 through the inhibition of Rheb, a Ras family GTPase (Inoki et al., 2003; Tee et al., 2003). Increased mTORC1 kinase activity likely underlies TSC pathophysiology and is a pathological hallmark of brain malformations in patients (Talos et al., 2008).

Deletion of *TSC1/2* in animal models affects a wide range of neuronal processes, and inhibition of mTORC1 corrects specific cellular, neuroanatomical, and neurological phenotypes (Meikle et al., 2007, 2008; Magri et al., 2011; Bateup et al., 2013; Tavazoie et al., 2005). The direct cellular and synaptic consequences of *TSC2* deletion in human neurons are unknown. Specifically, it is still unclear how increased TSC-mTORC1 pathway activity precipitates the onset of human neuronal dysfunction, how it alters multiple neurodevelopmental stages, and if and when phenotypes can be reversed.

Here, we used genome-engineered $TSC2^{+/-}$ and $TSC2^{-/-}$ human pluripotent stem cells to recapitulate the heterozygous loss of function underlying the disorder and study the effect of complete loss of *TSC2* in neuronal development, respectively. Combining a neuronal differentiation protocol and molecular, cellular, and electrophysiological analyses, our results reveal the effects of alterations of the TSC2-mTORC1 pathway on human neurodevelopment and synaptic physiology.

RESULTS

Generation of an Allelic Series of *TSC2* Deleted Human Embryonic Stem Cell Lines

Zinc-finger nuclease-mediated targeted gene disruption was used to generate heterozygous and homozygous deletions of *TSC2* in the well-characterized SA001 human embryonic stem cell (hESC) line (Englund et al., 2010), which we have previously used to study neuronal maturation (Dunkley et al., 2015). We generated an isogenic allelic series of *TSC2* deletions by inserting a neomycin selection cassette into one ($TSC2^{+/-}$) or both ($TSC2^{-/-}$) alleles or into the AAVS1 safe harbor locus ($TSC2^{+/+}$) (Figure 1A). Correct gene targeting was established by genomic PCR amplification across the disruption cassette (Figures S1A and S1B), and absence of additional genomic integrations was confirmed by targeted locus amplification (de Vree et al., 2014) (Figure S1C). Gene targeting resulted in decreased TSC2 protein levels in heterozygous lines and absence of the protein in homozygous clones (Figure 1B). To determine whether *TSC2* mutation affected mTORC1 function in hESCs, we monitored phosphorylation levels of the downstream substrate 40S ribosomal protein S6 (RPS6) and found increased phosphorylation in $TSC2^{-/-}$, but not $TSC2^{+/-}$, lines (Figure S1D). We observed no differences in hESC colony morphology (Figures 1C and S1E), proliferation, pluripotency, or spontaneous differentiation capacity (data not shown). These results suggest that *TSC2* deletion and mTORC1 hyperfunction do not grossly affect pluripotency of hESCs.

### Deletion of *TSC2* Causes Abnormal Structural Organization of Neuroectodermal Rosettes

In vivo, *Tsc2* ablation leads to embryonic lethality and defective neural tube closure in mouse embryos at E11.5 (Kobayashi et al., 1999). We therefore asked whether deletion of *TSC2* alters hu-man neuroectodermal rosette formation, the in vitro correlate of in vivo cortical neuroepithelium development (Shi et al., 2012). We induced neuroectodermal differentiation using a modified dual-SMAD inhibition protocol (Figure S2A; Experimental Procedures). Neuroepithelial progenitors expressed the forebrain rosette neural progenitor markers PLZF, Nestin, Pax6, and SOX1, suggesting efficient differentiation in control and mutant lines (Figures 1E and S2C; data not shown). The typical apicobasal polarity was mostly maintained in rosettes from all genotypes, as the tight junction protein zonula occludens 1 (ZO1) and M phase nuclei were oriented toward the lumen of the rosettes (Figures 1E and S2C) (Falk et al., 2012; Götz and Huttner, 2005). However, $TSC2^{-/-}$ rosettes were more heterogeneous in size due to formation of enlarged rosettes (Figures 1E, 1F, and S2D). Cell size was comparable across genotypes at this stage, suggesting that enlarged rosette size was likely due to increased cell number (Figure S2E). Importantly, this cellular phenotype correlated with overactivation of the mTORC1 pathway in $TSC2^{-/-}$ lines (Figure 1D). We conclude that biallelic *TSC2* deletion causes mTORC1 hyperfunction in neuroectodermal rosettes, which in turn impairs their structural organization.

Deletion of *TSC2* Alters Neuronal Proliferation, Differentiation, and Morphology in a Gene-Dosage-Dependent Manner

During early neuroectodermal specification, no alterations were observed in $TSC2^{+/-}$ lines. To investigate whether heterozygous *TSC2* loss of function, mimicking the TSC patient genotype, leads to neural dysfunction during later stages of development, we generated neural stem cells (NSCs) that can be differentiated into functional neurons (Figures S2A and S2F–S2J; see Experimental Procedures for details). To model a physiologically relevant neuronal network with excitatory and inhibitory neuronal connectivity, we utilized a protocol that differentiates NSCs to glutamatergic and GABAergic neurons (HuC/D+ cells, 50.9% ± 3.2%; GABA+/HuC/D+ cells, 11.3% ± 5.8% at day 28 of differentiation; Figures 2A, S2A, and S2B) (Dunkley et al., 2015).

TSC2 mutant lines showed early neuronal alterations. At day 14 of differentiation, $TSC2^{-/-}$ showed a ~55% reduction in the number of postmitotic (HuC/D+) neurons. The phenotype was less pronounced (~26% reduction) and transient in $TSC2^{+/-}$ lines (Figures 2B, 2C, and S3G). $TSC2^{-/-}$ cells exhibited reduced expression of neuronal progenitor markers and aberrant proliferation already 7 days of differentiation (Figures S3A–S3C). We investigated the potential mechanisms underlying the decreased neuronal content in $TSC2^{-/-}$ lines and found a small but significant increase in cell death of $TSC2^{-/-}$ neurons at day 7 of differentiation (Figure S3E). In addition, TSC2$^{-/-}$ lines showed an increased differentiation toward the astroglial lineage, as shown by upregulation of the astroglia marker NFIA and increase in GFAP+ cells at late stages of differentiation (Figures S3D, S2L, and S2M). To understand the molecular correlates of the observed alterations in neuronal differentiation, we studied the expression of several genes and proteins relevant to neuronal development (Tables S1 and S2). $TSC2^{+/-}$ and $TSC2^{-/-}$ immature neurons showed increased expression of neural stem cell and proliferation markers (*SOX2*, *NESTIN*, and *PCNA*) and a concomitant downregulation of genes associated with neuronal
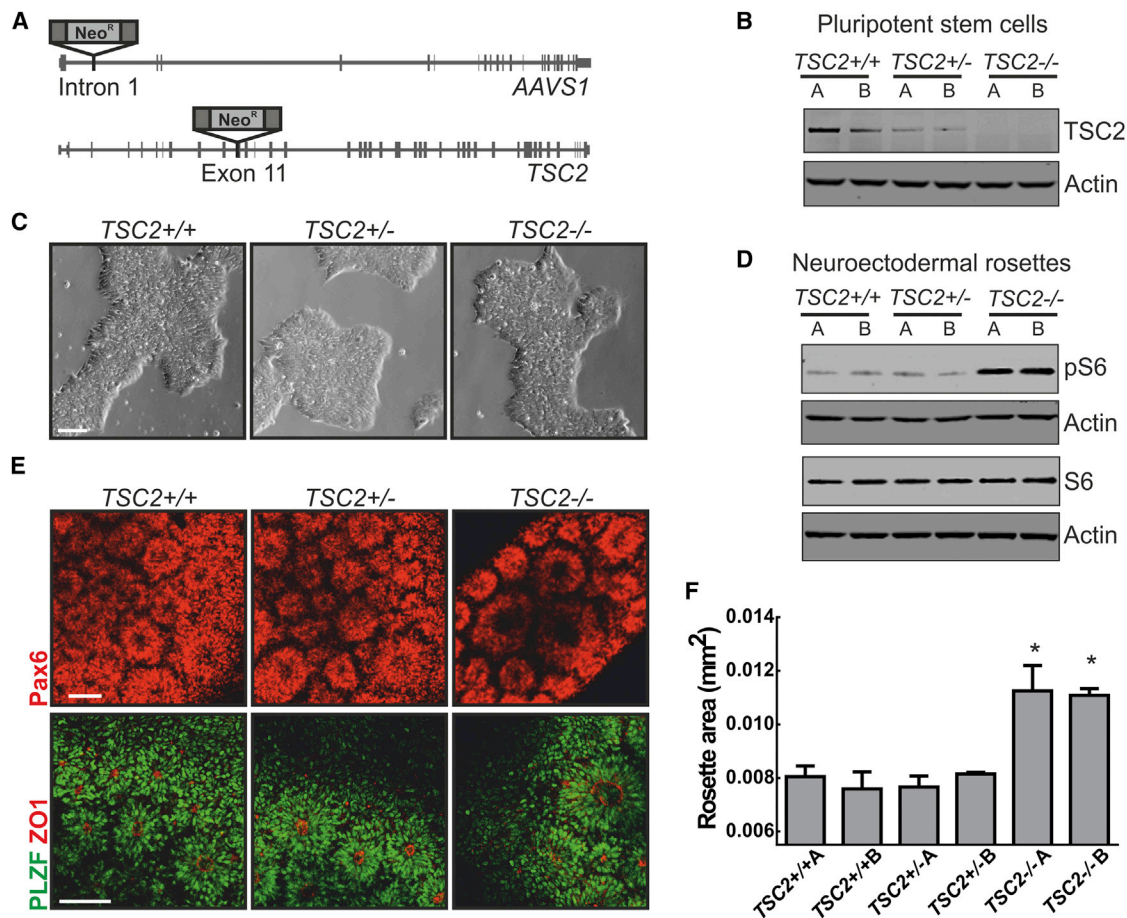
Figure 1. *TSC2* Deletion Leads to mTORC1 Hyperfunction and Altered Structural Organization of Neuroectodermal Rosettes
(A) Gene targeting strategy using zinc-finger nucleases. For control lines (*TSC2*$^{+/+}$), a neomycin resistance cassette was inserted into intron 1 of one allele of the *AAVS1* (*PPP1R12C*) locus. For *TSC2*$^{+/−}$ and *TSC2*$^{−/−}$ lines the selection cassette was inserted in exon 11 of one or both alleles of *TSC2,* respectively.
(B and D) Proteins from hESCs (25 μg; B) and 3-day-old neural rosettes (12.5 μg; D) were analyzed by SDS-PAGE/immunoblotting.
(C) Representative bright-field images of hESC clonal isolates. Scale bar, 100 μm.
(E) Confocal images of 2.5-day-old neural rosettes. Confocal z-axis stacks were acquired and reconstructed. Scale bars, 100 μm.
(F) Size of 2.5-day-old rosettes. Data represent median ± SEM of three independent derivations, p < 0.05 *TSC2*$^{−/−}$ versus *TSC2*$^{+/+}$ and *TSC2*$^{+/−}$.
(B, D, and F) A and B indicate two clones with the same genotype. See also Figures S1 and S2.

maturation and synapse formation. Intriguingly, we observed dysregulation of the chloride transporters *NKCC1* (*SLC12A2*) and *KCC2* (*SLC12A5*), which affect neuronal excitability in response to GABA, are dynamically regulated during brain development and are altered in cortical tubers from TSC patients (Figures 2E and S3F) (Ben-Ari et al., 2012; Jagasia et al., 2009; Talos et al., 2012). At day 14 of differentiation, *TSC2*$^{−/−}$ (but not *TSC2*$^{+/−}$) neurons showed increased soma size, recapitulating what is observed in cortical tubers and attributed to mTORC1 hyperfunction (Figure 2B, right; and Figure 2D) (Ruppe et al., 2014). To assess morphological alterations in mature neurons (Figures S2K and S2N), we analyzed biocytin-filled 6- to 8-week-old neurons (Figure 2F). *TSC2*$^{−/−}$ neurons exhibited increased dendritic arborization measured by Sholl analysis, increased soma size, and an ∼2-fold increase in total dendritic length (Figures 2G, S3H, and S3I). *TSC2*$^{+/−}$ neurons did not show gross morphological changes. In a correlation analysis,

we observed a positive correlation of moderated *t* statistics values for transcripts and proteins between *TSC2*$^{+/−}$ and *TSC2*$^{−/−}$ lines compared to controls at days 14 and 41 of differentiation (r = 0.617 and r = 0.298 for transcripts and r = 0.552 and r = 0.444 for proteins at days 14 and 41, respectively; Figure 2H). Cluster analysis revealed a trend toward downregulation of genes relevant for synaptic transmission in both *TSC2*$^{+/−}$ and *TSC2*$^{−/−}$ neurons. The cluster of proteins/transcripts with the largest effect included genes and pathways associated with autism including *CNTNAP2*, *NLG3*, and *KCC2* (Figure 2I). In addition, we observed in both genotypes downregulation of RBFOX1, a splicing factor reduced in brains from idiopathic ASD patients (Figure S3J) (Fogel et al., 2012, Voineagu et al., 2011). In the aggregate, these data indicate that monoallelic deletion of *TSC2* causes persistent dysregulation of ASD-relevant genes that is similar to that observed in *TSC2*$^{−/−}$ cells but whose extent remains below the threshold required to elicit
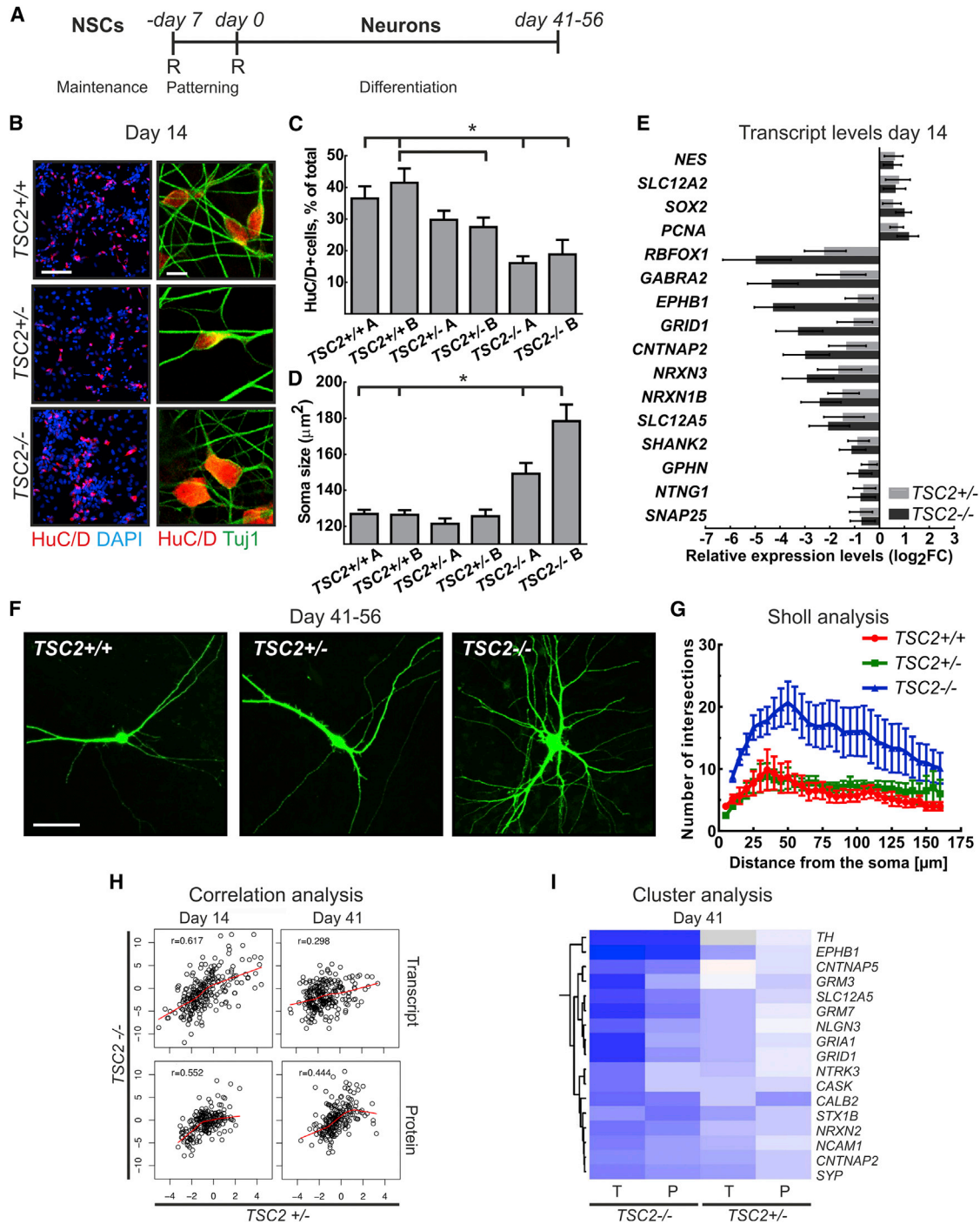
Figure 2. *TSC2* Deletion Causes Deficits in Neuronal Proliferation, Differentiation, and Maturation

(A) Neuronal differentiation protocol outline. NSCs, neural stem cells; R, replating. For details, see Experimental Procedures.

(B) Representative confocal images of day 14 differentiated neurons. Confocal z-axis stacks were acquired and reconstructed. Scale bars represent 100 μm (left) and 10 μm (right).

(C and D) Neuronal content (C) and soma size (HuC/D+ area; D) in day 14 differentiated cultures. Experiments were as in (B); n = 4, *p < 0.05. Acquisition and automated quantification performed with Operetta HCS. Data represent mean ± SEM. A and B indicate two clones with the same genotypes.

(E) qPCR quantitation of gene expression levels in day 14 differentiated cultures. Data are normalized to a pool of housekeeping genes and expressed as fold change ($\log_2$) relative to *TSC2*^{+/+} lines. Data represent mean ± 95% confidence interval, n ≥ 4. All fold changes are statistically significant.

(F) Representative fluorescence images of biocytin-filled day 41–63 differentiated neurons. Confocal images were acquired with Zen software. Scale bar, 50 μm.

(G) Sholl analysis of experiments as in (F). *TSC2*^{+/+}: n = 6, *TSC2*^{+/−}: n = 4, *TSC2*^{−/−}: n = 8. Data represent mean ± SEM.

(legend continued on next page)
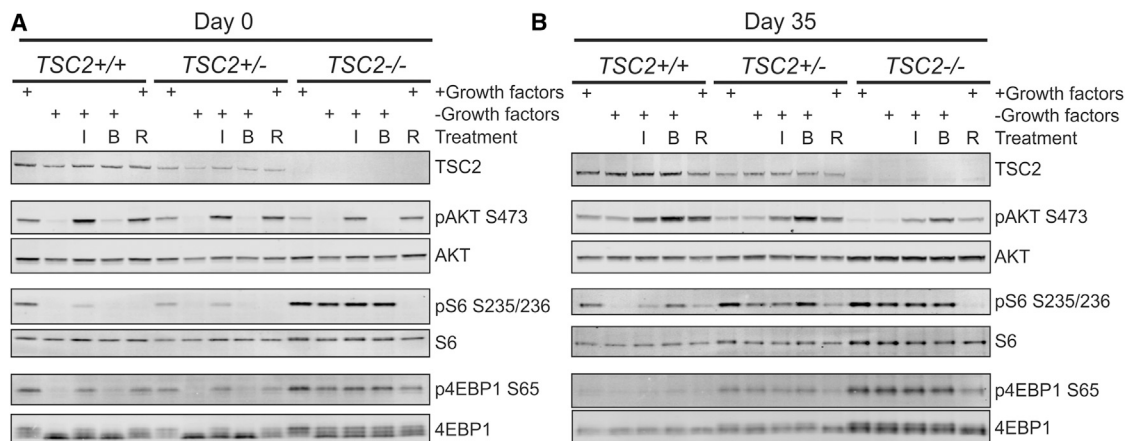
Figure 3. Neuronal Maturation Reveals mTORC1 Hyperfunction in $TSC2^{+/-}$ Neurons

(A and B) Proteins (10 μg) from NSCs (A) and day 35 differentiated neurons (B) were analyzed by SDS-PAGE/immunoblotting. Where indicated, cells were treated as follows: FEB (+ growth factors day 0) or BGAA (+ growth factors day 35) medium overnight; R, 50 nM rapamycin for 1.5 hr; starvation in Neurobasal medium (− growth factors) for 5 hr; IGF1 (10 ng/ml) (I) or BDNF (20 ng/ml) (B) for 30 min. DMSO was vehicle control in untreated cells. See also Figure S4.

most of the early cellular phenotypes seen in the full knockout. In addition, our molecular analysis suggests that *TSC2* deletion leads to alterations in synapse biology in both genotypes.

TSC2 Heterozygous Deletion Leads to mTORC1 Hyperfunction in Differentiating Neuronal Cultures

To address whether the observed molecular and cellular deficits correlated with alterations in mTOR signaling, we monitored the phosphorylation status of mTORC1 downstream substrates in response to physiologically relevant modulators (insulin-like growth factor [IGF] and brain-derived neurotrophic factor [BDNF]) and known inhibitors (rapamycin and nutrient starvation) of the pathway. As expected, TSC2 protein was reduced to ~50% in *TSC2*+/− lines and absent in *TSC2*−/− lines (Figures S4A and S4B). Lines from all genotypes exhibited an IGF1-dependent increase in phosphorylation of the mTORC2 substrate AKT at serine 473 (Sarbassov et al., 2005) in both NSCs (Figures 3A and S4E) and neurons (Figures 3B and S4F). In contrast, BDNF elicited a response only in neurons, consistent with functional maturation of the culture (Figures 3A, 3B, S4C, and S4D). Phosphorylation of mTORC1 targets S6 and eukaryotic translation initiation factor 4E binding protein 1 (4EBP1) showed *TSC2* gene-dosage-dependent alterations. *TSC2*−/− cells showed constitutive activation of mTORC1 as shown by increased phosphorylation of S6 and 4EBP1 even upon withdrawal of growth factors, a condition which silences the pathway in control lines. Furthermore, *TSC2*−/− lines exhibited a marked reduction of AKT phosphorylation, previously ascribed to mTORC1-dependent negative feedback signaling (Shah and

Hunter, 2006, Harrington et al., 2004). Indeed, the reduction was partially reverted upon rapamycin treatment (from ~34% to ~84% of *TSC2*+/+ at day 0 and from ~12% to ~42% of *TSC2*+/+ at day 35, in the presence of growth factors without and with rapamycin, respectively; Figures 3A, 3B, and S4H). Surprisingly, although we could not observe gross differential regulation between control and *TSC2*+/− lines at the NSC stage (Figure 3A), phosphorylation of S6 and 4EBP1 was increased in *TSC2*+/− lines at day 35 (Figures 3B and S4D; quantification in Figure S4H).

Interestingly, upon differentiation, negative regulators of the mTOR pathway were upregulated in control lines (TSC1 and TSC2, ~3-fold; PTEN, ~10-fold), suggesting a tight regulation of the pathway in neurons (Figures S4A and S4B). In mature neurons, TSC1 protein expression was reduced in *TSC2*+/− and *TSC2*−/− lines (Figures S4A and S4B). This suggests that the mTORC1 pathway is tightly regulated during neuronal maturation and that an ~50% reduction in *TSC2* leads to a molecular phenotype in neurons. Moreover, homozygous deletion of TSC2 leads to constitutive activation of mTORC1 and dysregulation of feedback signaling pathways as observed in cortical tubers (Ruppe et al., 2014).

mTORC1 Inhibition Corrects Excitability and Synaptogenesis Deficits Independently of Early Neurodevelopmental Alterations

We next asked if, and at what stage during neuronal differentiation, cellular and electrophysiological phenotypes could be corrected by inhibition of mTORC1. Rapamycin treatment of

(H) Correlation analysis between *TSC2*+/− and *TSC2*−/− lines of *t* statistics values compared to *TSC2*+/+ lines calculated for 254 transcripts and 196 proteins at day 14 and day 41 of differentiation. Pearson correlation values are indicated. Red line is calculated using LOWESS smooth splines.

(I) Cluster analysis (using Euclidean distance and Ward clustering) based on the *t* statistics representing significance of change relative to wild-type (WT) for both genotypes at day 41. Analysis on genes for which both protein (P) and transcript (T) measurements were available. A sub-cluster around EPHB1 showed very marked and consistent effects.

See also Figures S2 and S3 and Tables S1 and S2.
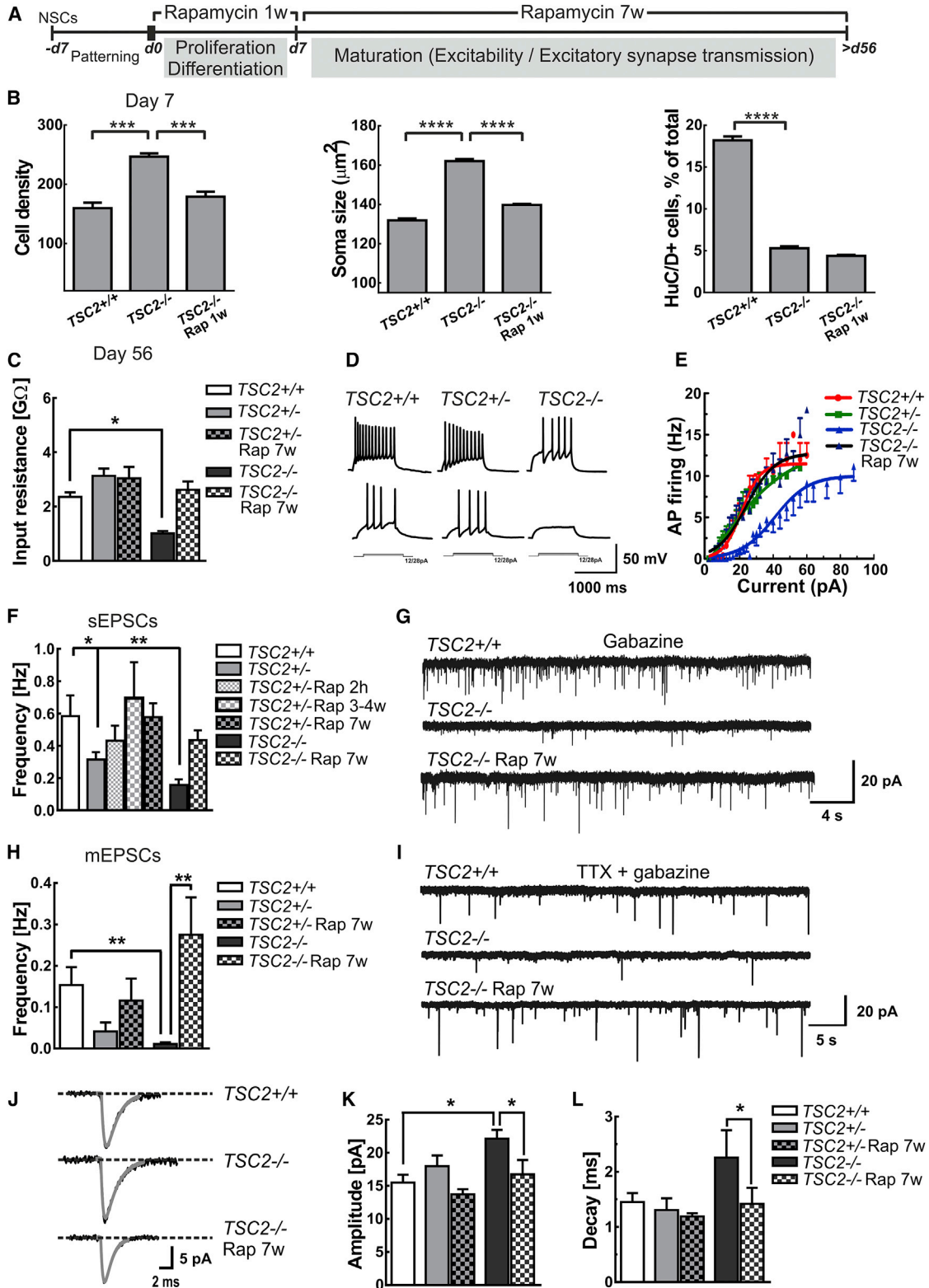
$TSC2^{-/-}$ NSCs during the first 7 days of differentiation reverted cell density and soma size to control levels but failed to correct the deficit in neuronal differentiation (Figures 4A and 4B). The latter phenotype was partially ameliorated when the treatment was applied on proliferating NSCs during the patterning stage, suggesting that earlier application of rapamycin during neuroectodermal differentiation might be beneficial (Figure S4I).

In mature neurons, whole-cell patch-clamp recordings revealed that $TSC2^{-/-}$ neurons had an ~50% reduction in electrical input resistance and an ~2-fold increase in membrane capacitance (Figures 4C and S4J), which correlated with increased total dendritic length of individual cells (Figure S4K). Normalizing the input conductance by the capacitance in individual cells revealed no significant differences between genotypes, indicating that the conductance density of open ion channels at the resting membrane potential was not significantly different (data not shown) and suggesting that the alterations in passive membrane properties are likely due to increased cell size. Since the increased capacitance and decreased input resistance might impact electrical excitability, we measured action potential (AP) firing in response to 1-s current pulses with increasing current amplitudes. While $TSC2^{+/-}$ neurons responded similarly to control cells, $TSC2^{-/-}$ neurons required a 2-fold-larger current amplitude to generate the same frequency of AP firing (Figures 4D and 4E). Similar results were obtained when measuring the AP firing probability in response to brief 10-ms current pulses with increasing amplitude (Figures S4L and S4M). The functional properties of voltage-gated sodium and potassium channels were unlikely to be different, since the shapes of individual APs were indistinguishable across genotypes (Figures S4N–S4P). To test whether changes in electrical excitability were due to enhanced mTORC1 activity, we treated cells for 7 weeks with 2 nM rapamycin, a concentration that inhibits mTORC1 signaling (Figure S4G), starting at day 7, after early neuronal differentiation had occurred. Remarkably, after treatment, both passive membrane properties and AP firing were indistinguishable from control (Figures 4C–4E, S4J, and S4L).

Our molecular analysis suggested alterations in excitatory synaptic function in $TSC2^{+/-}$ and $TSC2^{-/-}$ neurons (Figure 2I). To analyze glutamatergic synapse formation and excitatory synaptic transmission, we recorded spontaneous excitatory synaptic currents (sEPSCs) and miniature excitatory synaptic currents (mEPSCs) in the presence of the GABA$_A$-receptor antagonist gabazine (4 μM). The frequency of sEPSCs (0.57 $\pm$ 0.15Hz, n = 12, control) was significantly reduced in $TSC2^{+/-}$ as well as in $TSC2^{-/-}$ neurons relative to control lines in a gene-dosage-dependent manner (0.28 $\pm$ 0.05 Hz, p < 0.05, n = 24 and 0.16 $\pm$ 0.04 Hz, p < 0.01, n = 11, respectively; Figures 4F and 4G). The phenotype was reverted by long-term (7 weeks starting at day 7 of differentiation), but not acute (2 hr starting at 8 weeks of differentiation), treatment with rapamycin. To understand whether the phenotype could be rescued at late developmental stage by longer treatment, we applied rapamycin for 3–4 weeks starting at 6 weeks of differentiation. The treatment fully corrected the deficit in sEPSCs frequency ($TSC2^{+/-}$ with 3- to 4-week rapamycin: 0.69 $\pm$ 0.22 Hz, n = 7). To test whether the reduction in frequency of sEPSCs was caused by decreased excitability or a reduced number of synaptic connections, we recorded mEPCs in the presence of 0.5 μM TTX. Similarly to spontaneous synaptic currents, mEPSC frequency (0.15 $\pm$ 0.04 Hz, n = 24) was reduced in mutant neurons ($TSC2^{+/-}$: 0.04 $\pm$ 0.02 Hz, n = 7; $TSC2^{-/-}$: 0.01 $\pm$ 0.01 Hz, n = 11), indicating a reduced number of glutamatergic synapses, and the phenotype was corrected by chronic rapamycin treatment (Figures 4H and 4I). Furthermore, rapamycin could correct the slight but significant increase in the amplitude and decay time course of average mEPSCs in $TSC2^{-/-}$ neurons (Figures 4J–4L).

Taken together, these data show that neuronal and synaptic alterations, including a deficit in glutamatergic synaptic transmission, are triggered in a $TSC2$-gene-dosage-dependent manner and can be corrected by pharmacological mTORC1 inhibition. Importantly, synaptic defects are corrected even when rapamycin treatment is started after the establishment of synaptic network connectivity.

Figure 4. Reversal of Neurodevelopmental and Synaptogenesis Deficits by mTORC1 Inhibition

(A) Outline of phenotypic reversal experiments with rapamycin treatment. NSCs, neural stem cells.

(B) Cell density (DAPI+ nuclei/field), neuronal soma size (HuC/D+ area), and neuronal content (% of HuC/D+ cells / DAPI+ nuclei). Data represent mean $\pm$ SEM. Untreated: ten wells/plate, 27 fields/well, four plates; treated: three wells, 27 fields/well. ***p < 0.001, ****p < 0.0001.

(C) Input resistance of day 56–63 differentiated neurons untreated or treated with 2 nM rapamycin for 7 weeks. $TSC2^{+/+}$: n = 37, $TSC2^{+/-}$: untreated n = 39, treated n = 4; $TSC2^{-/-}$: untreated n = 31, treated n = 27.

(D) Representative recordings of action potentials (AP) induced by somatic current injections of 18 and 28 pA.

(E) AP firing frequency-current relationship calculated from recordings of action potentials induced by a 1-s pulse of somatic current injections ΔI = 2 pA. Curve was constructed using Boltzmann sigmoidal fit in GraphPad Prism.

(F) Frequency of spontaneous EPSCs (5-min recording in the presence of 4 μM gabazine). $TSC2^{+/+}$: n = 12; $TSC2^{+/-}$: untreated n = 24, treated for 2 hr with 20 nM rapamycin n = 12, treated with 2 nM rapamycin for 3–4 weeks n = 7 or for 7 weeks n = 12; $TSC2^{-/-}$: untreated n = 11, treated with 2 nM rapamycin for 7 weeks n = 10.

(G) Representative traces of sEPSCs quantified in (F).

(H) Frequency of mEPSC in day 56 - 63 differentiated neurons untreated or treated with 2 nM rapamycin for 7 weeks. $TSC2^{+/+}$: n = 24; $TSC2^{+/-}$: untreated n = 7, treated n = 5; $TSC2^{-/-}$: untreated n = 11, treated n = 12.

(I) Representative traces of mEPSCs quantified in (H) recorded in the presence of 0.5 μM TTX and 4 μM gabazine.

(J) Representative traces of mEPSCs. Black line represents the average of 25 single events. Gray line represents the biexponential fit of the average trace.

(K) Amplitudes of mEPSCs in neurons untreated or treated with 2 nM rapamycin for 7 weeks. $TSC2^{+/+}$: n = 18; $TSC2^{+/-}$: untreated n = 5, treated n = 4; $TSC2^{-/-}$: untreated n = 5, treated n = 6.

(L) Decay time constants of mEPSCs in neurons untreated or treated with 2 nM rapamycin for 7 weeks. $TSC2^{+/+}$: n = 18; $TSC2^{+/-}$: untreated n = 5, treated n = 4; $TSC2^{-/-}$: untreated n = 5, treated n = 6.

Bar graphs represent mean $\pm$ SEM (C, E, F, H, K, and L); *p < 0.05; **p < 0.01. See also Figure S4.

DISCUSSION

The pathophysiological mechanisms underlying neuroanatomical and neurological alterations in patients affected by TSC are largely unknown. Here, we show that *TSC2* deletion leads to exaggerated mTORC1 signaling during differentiation of human neurons in a gene-dosage-dependent manner, and this correlates with molecular and cellular alterations at multiple developmental stages. We show that *TSC2* deletion alters the structure of human neuroectodermal rosettes, providing an in vitro correlate of neural tube formation deficits observed during in vivo embryonic development. Interestingly, abnormal rosette organization has been recently reported in hiPSCs carrying 15q11.2 microdeletion, a risk factor for schizophrenia and autism, supporting a role for early neurodevelopmental defects in neuropsychiatric disorders (Yoon et al., 2014). At later stages, we show that heterozygous loss of *TSC2* results in a transient delay in early neuronal differentiation. Deficits in neuronal differentiation have been suggested to lead to abnormal brain wiring and could contribute to the altered connectivity observed in TSC patients (Krishnan et al., 2010; La Fata et al., 2014; Baumer et al., 2015). Furthermore, we demonstrate that heterozygous and homozygous loss of *TSC2* leads to altered synaptogenesis and transmission. By inhibiting mTORC1 at different developmental stages, we show that early neurodevelopment and synaptogenesis can be uncoupled and corrected independently of each other. Indeed, excitatory synapse reduction can be corrected in both genotypes by long-term mTORC1 inhibition even after the onset of early differentiation deficits. Importantly, the correction is achieved even when the treatment is started at late differentiation stages, after synaptic network connectivity has been established.

Cortical tubers are a common neuropathological feature in TSC patients and their role in epilepsy and cognitive impairment is under close scrutiny (Jansen et al., 2007, 2008; Doherty et al., 2005; Major et al., 2009). We show that homozygous deletion of *TSC2* recapitulates molecular, cellular, and electrophysiological features observed in dysplastic neurons from cortical tubers. Notably, alterations are dependent on mTORC1-hyperactivity, as they can be corrected by rapamycin treatment. Extending the functional characterization of our *TSC2* mutant neurons will contribute to understand the role of altered mTORC1 signaling, excitability, and synaptic connectivity in the onset of neuronal network dysfunction and of epilepsy, a pathological feature associated with TSC and involved in the development of ASD.

Patients affected by TSC present with autism (50%) and comorbid symptoms including epilepsy (80%–90%) and varying degrees of intellectual disability (45%) (Jeste et al., 2008; Crino et al., 2006; Curatolo and Bombardieri, 2008). ASD is characterized by a remarkable heterogeneity in genetic causes and clinical manifestations. Consequently, identifying convergence in ASD biology remains an elusive challenge. Using TSC as a model of monogenic forms of ASD, we have characterized phenotypes in human neurons including deficits in synaptogenesis and alterations in pathways and genes previously associated with ASD. Extending this analysis to multiple genetically defined models of ASD will provide an unprecedented opportunity to link human genetics to neuronal phenotypes and potentially identify shared pathophysiological mechanisms.

EXPERIMENTAL PROCEDURES

Genome Editing

Plasmids encoding zinc-finger nucleases (ZFNs) targeting exon 11 of *TSC2* (CompoZr knockout ZFN) and mRNA encoding ZFNs targeting exon 1 of the *PPP1R12C* locus (CompoZr Targeted Integration Kit) were from Sigma. Targeting constructs harboring a *loxP*-flanked PGK promoter-driven neomycin phosphotransferase cassette surrounded by sequences homologous to the genomic locus adjacent to the ZFN cut sites were synthesized de novo. Constructs were electroporated into SA001 hESCs, which were selected with 0.2 µg/ml G418 (Life Technologies), and clones with site-specific cassette insertions were identified by PCRs from genomic DNA. For more detail, refer to Supplemental Experimental Procedures.

Neuronal Differentiation

For patterning, NSCs were plated on polyornithin-/laminin-coated dishes at 10,000–15,000 cells/cm² in basal medium with 100 ng/ml FGF-8 (Peprotech), 200 ng/ml sonic hedgehog (Peprotech), and 100 µM ascorbic acid 2-phosphate (Sigma) and cultured for 1 week. For differentiation, the resultant progenitors were plated at 35,000–50,000 cells/cm² in basal medium with 20 ng/ml BDNF, 10 ng/ml glial cell-derived neurotrophic factor (GDNF; Peprotech), 500 µM dibutyryl cyclic AMP (Sigma), and 100 µM ascorbic acid 2-phosphate. For more detail, refer to Supplemental Experimental Procedures.

Electrophysiology

Recordings were performed at 22°C–24°C. Cells were superfused with ACSF containing (in mM): 123 NaCl, 25 D-Glucose, 10 HEPES, 25 NaHCO₃, 5 KCl, 1 NaH₂PO₄, 2 CaCl₂ and 1 MgCl₂. Internal solution contained (in mM): 140 KCl, 10 EGTA, 10 HEPES, 2 MgCl₂, 2 Na₂ATP, 1 Phosphocreatine and 0.3 NaGTP with a pH of 7.28. Gluconate-based solution contained 135 mM K-gluconate, 20 mM KCl, 10 mM HEPES, 0.1 mM EGTA, 2 mM MgCl₂, 2 mM Na₂ATP, 1 mM phosphocreatine, and 0.3 mM NaGTP. Borosilicate glass patch pipettes (2.5–4.0 MΩ) were used. Cells were patched in the whole-cell configuration with a stable series resistance of $R_S < 20$ MΩ. sEPSCs and mEPSCs were recorded at a membrane potential of −70 mV in voltage-clamp mode. APs were elicited in current-clamp mode via current injections of either 1 s or 20 pulses of 10 ms duration. For more detail, refer to Supplemental Experimental Procedures.

Imaging

Fluorescent images were acquired using a Leica TCS SP5 (Leica Microsystems) inverted microscope, Opera High Content Screening System (Perkin Elmer) or Operetta High Content Imaging System (PerkinElmer). For data analysis, refer to Supplemental Experimental Procedures.

Western Blot

Protein samples were resolved on NuPAGE 4%–12% gels and transferred to nitrocellulose membranes using the iBlot Dry Blotting System (Life Technologies). Blot scans were acquired using a Li-COR scanner (Odyssey) and analyzed using the Image Studio Software (Li-COR Biosciences). Antibodies are listed in Supplemental Experimental Procedures.

Transcriptome Analysis

Real-time qPCR was performed with TaqMan Gene Expression assays (Life Technologies) using a 96.96 Dynamic Array (Fluidigm). For data analysis, refer to Supplemental Experimental Procedures.

Mass Spectrometry

Experiments and peak selection were performed as described previously (Dunkley et al., 2015). For data analysis, refer to Supplemental Experimental Procedures.

SUPPLEMENTAL INFORMATION

AUTHOR CONTRIBUTIONS

V.C., S.A., and M.V. designed, conducted, and analyzed experiments and wrote the manuscript. V.C. performed cellular and molecular analyses. S.A. generated genome-edited lines and performed cellular and molecular analyses. M.V. and K.B. performed all the electrophysiological analyses and the biocytin-based morphological analysis. E.S., A.F., T.D., S.Z., S.L., C.P., L.C.-G., M.B., and A.K. performed experiments and analyzed data. M.E., C.M., F.K., P.P., and F.F. analyzed data. M.G., S.J., and A.G. provided scientific and experimental input. J.B. and R.J. designed the study, analyzed data, and wrote the manuscript.

CONFLICTS OF INTEREST

ACKNOWLEDGMENTS

REFERENCES

Bateup, H.S., Johnson, C.A., Denefrio, C.L., Saulnier, J.L., Kornacker, K., and Sabatini, B.L. (2013). Excitatory/inhibitory synaptic imbalance leads to hippocampal hyperexcitability in mouse models of tuberous sclerosis. Neuron *78*, 510–522.

Baumer, F.M., Song, J.W., Mitchell, P.D., Pienaar, R., Sahin, M., Grant, P.E., and Takahashi, E. (2015). Longitudinal changes in diffusion properties of white matter pathways of children with tuberous sclerosis complex. Pediatr. Neurol. *52*, 615–623.

Ben-Ari, Y., Khalilov, I., Kahle, K.T., and Cherubini, E. (2012). The GABA excitatory/inhibitory shift in brain maturation and neurological disorders. Neuroscientist *18*, 467–486.

Bourgeron, T. (2009). A synaptic trek to autism. Curr. Opin. Neurobiol. *19*, 231–234.

Cepeda, C., André, V.M., Hauptman, J.S., Yamazaki, I., Huynh, M.N., Chang, J.W., Chen, J.Y., Fisher, R.S., Vinters, H.V., Levine, M.S., and Mathern, G.W. (2012). Enhanced GABAergic network and receptor function in pediatric cortical dysplasia Type IIB compared with tuberous sclerosis complex. Neurobiol. Dis. *45*, 310–321.

Chan, J.A., Zhang, H., Roberts, P.S., Jozwiak, S., Wieslawa, G., Lewin-Kowalik, J., Kotulska, K., and Kwiatkowski, D.J. (2004). Pathogenesis of tuberous sclerosis subependymal giant cell astrocytomas: biallelic inactivation of TSC1 or TSC2 leads to mTOR activation. J. Neuropathol. Exp. Neurol. *63*, 1236–1242.

Crino, P.B., Nathanson, K.L., and Henske, E.P. (2006). The tuberous sclerosis complex. N. Engl. J. Med. *355*, 1345–1356.

Crino, P.B., Aronica, E., Baltuch, G., and Nathanson, K.L. (2010). Biallelic TSC gene inactivation in tuberous sclerosis complex. Neurology *74*, 1716–1723.

Curatolo, P., and Bombardieri, R. (2008). Tuberous sclerosis. Handb. Clin. Neurol. *87*, 129–151.

de Vree, P.J., de Wit, E., Yilmaz, M., van de Heijning, M., Klous, P., Verstegen, M.J., Wan, Y., Teunissen, H., Krijger, P.H., Geeven, G., et al. (2014). Targeted sequencing by proximity ligation for comprehensive variant detection and local haplotyping. Nat. Biotechnol. *32*, 1019–1025.

Doherty, C., Goh, S., Young Poussaint, T., Erdag, N., and Thiele, E.A. (2005). Prognostic significance of tuber count and location in tuberous sclerosis complex. J. Child Neurol. *20*, 837–841.

Dunkley, T., Costa, V., Friedlein, A., Lugert, S., Aigner, S., Ebeling, M., Miller, M.T., Patsch, C., Piraino, P., Cutler, P., and Jagasia, R. (2015). Characterization of a human pluripotent stem cell-derived model of neuronal development using multiplexed targeted proteomics. Proteomics Clin. Appl. *9*, 684–694.

Englund, M.C., Caisander, G., Noaksson, K., Emanuelsson, K., Lundin, K., Bergh, C., Hansson, C., Semb, H., Strehl, R., and Hyllner, J. (2010). The establishment of 20 different human embryonic stem cell lines and subclones; a report on derivation, culture, characterisation and banking. In Vitro Cell. Dev. Biol. Anim. *46*, 217–230.

Falk, A., Koch, P., Kesavan, J., Takashima, Y., Ladewig, J., Alexander, M., Wiskow, O., Tailor, J., Trotter, M., Pollard, S., et al. (2012). Capture of neuroepithelial-like stem cells from pluripotent stem cells provides a versatile system for in vitro production of human neurons. PLoS ONE *7*, e29597.

Fogel, B.L., Wexler, E., Wahnich, A., Friedrich, T., Vijayendran, C., Gao, F., Parikshak, N., Konopka, G., and Geschwind, D.H. (2012). RBFOX1 regulates both splicing and transcriptional networks in human neuronal development. Hum. Mol. Genet. *21*, 4171–4186.

Gkogkas, C.G., Khoutorsky, A., Ran, I., Rampakakis, E., Nevarko, T., Weatherill, D.B., Vasuta, C., Yee, S., Truitt, M., Dallaire, P., et al. (2013). Autism-related deficits via dysregulated eIF4E-dependent translational control. Nature *493*, 371–377.

Götz, M., and Huttner, W.B. (2005). The cell biology of neurogenesis. Nat. Rev. Mol. Cell Biol. *6*, 777–788.

Harrington, L.S., Findlay, G.M., Gray, A., Tolkacheva, T., Wigfield, S., Rebholz, H., Barnett, J., Leslie, N.R., Cheng, S., Shepherd, P.R., et al. (2004). The TSC1-2 tumor suppressor controls insulin-PI3K signaling via regulation of IRS proteins. J. Cell Biol. *166*, 213–223.

Henske, E.P., Wessner, L.L., Golden, J., Scheithauer, B.W., Vortmeyer, A.O., Zhuang, Z., Klein-Szanto, A.J., Kwiatkowski, D.J., and Yeung, R.S. (1997). Loss of tuberin in both subependymal giant cell astrocytomas and angiomyolipomas supports a two-hit model for the pathogenesis of tuberous sclerosis tumors. Am. J. Pathol. *151*, 1639–1647.

Inoki, K., Li, Y., Xu, T., and Guan, K.L. (2003). Rheb GTPase is a direct target of TSC2 GAP activity and regulates mTOR signaling. Genes Dev. *17*, 1829–1834.

Jagasia, R., Steib, K., Englberger, E., Herold, S., Faus-Kessler, T., Saxe, M., Gage, F.H., Song, H., and Lie, D.C. (2009). GABA-cAMP response element-binding protein signaling regulates maturation and survival of newly generated neurons in the adult hippocampus. J. Neurosci. *29*, 7966–7977.

Jansen, F.E., van Huffelen, A.C., Algra, A., and van Nieuwenhuizen, O. (2007). Epilepsy surgery in tuberous sclerosis: a systematic review. Epilepsia *48*, 1477–1484.

Jansen, F.E., Vincken, K.L., Algra, A., Anbeek, P., Braams, O., Nellist, M., Zonnenberg, B.A., Jennekens-Schinkel, A., van den Ouweland, A., Halley, D., et al. (2008). Cognitive impairment in tuberous sclerosis complex is a multifactorial condition. Neurology *70*, 916–923.

Jeste, S.S., Sahin, M., Bolton, P., Ploubidis, G.B., and Humphrey, A. (2008). Characterization of autism in young children with tuberous sclerosis complex. J. Child Neurol. *23*, 520–525.

Kobayashi, T., Minowa, O., Kuno, J., Mitani, H., Hino, O., and Noda, T. (1999). Renal carcinogenesis, hepatic hemangiomatosis, and embryonic lethality caused by a germ-line Tsc2 mutation in mice. Cancer Res. 59, 1206–1211.

Krishnan, M.L., Commowick, O., Jeste, S.S., Weisenfeld, N., Hans, A., Gregas, M.C., Sahin, M., and Warfield, S.K. (2010). Diffusion features of white matter in tuberous sclerosis with tractography. Pediatr. Neurol. 42, 101–106.

La Fata, G., Gärtner, A., Domínguez-Iturza, N., Dresselaers, T., Dawitz, J., Poorthuis, R.B., Averna, M., Himmelreich, U., Meredith, R.M., Achsel, T., et al. (2014). FMRP regulates multipolar to bipolar transition affecting neuronal migration and cortical circuitry. Nat. Neurosci. 17, 1693–1700.

Magri, L., Cambiaghi, M., Cominelli, M., Alfaro-Cervello, C., Cursi, M., Pala, M., Bulfone, A., Garcìa-Verdugo, J.M., Leocani, L., Minicucci, F., et al. (2011). Sustained activation of mTOR pathway in embryonic neural stem cells leads to development of tuberous sclerosis complex-associated lesions. Cell Stem Cell 9, 447–462.

Major, P., Rakowski, S., Simon, M.V., Cheng, M.L., Eskandar, E., Baron, J., Leeman, B.A., Frosch, M.P., and Thiele, E.A. (2009). Are cortical tubers epileptogenic? Evidence from electrocorticography. Epilepsia 50, 147–154.

Meikle, L., Talos, D.M., Onda, H., Pollizzi, K., Rotenberg, A., Sahin, M., Jensen, F.E., and Kwiatkowski, D.J. (2007). A mouse model of tuberous sclerosis: neuronal loss of Tsc1 causes dysplastic and ectopic neurons, reduced myelination, seizure activity, and limited survival. J. Neurosci. 27, 5546–5558.

Meikle, L., Pollizzi, K., Egnor, A., Kramvis, I., Lane, H., Sahin, M., and Kwiatkowski, D.J. (2008). Response of a neuronal model of tuberous sclerosis to mammalian target of rapamycin (mTOR) inhibitors: effects on mTORC1 and Akt signaling lead to improved survival and function. J. Neurosci. 28, 5422–5432.

Qin, W., Chan, J.A., Vinters, H.V., Mathern, G.W., Franz, D.N., Taillon, B.E., Bouffard, P., and Kwiatkowski, D.J. (2010). Analysis of TSC cortical tubers by deep sequencing of TSC1, TSC2 and KRAS demonstrates that small second-hit mutations in these genes are rare events. Brain Pathol. 20, 1096–1105.

Rosser, T., Panigrahy, A., and McClintock, W. (2006). The diverse clinical manifestations of tuberous sclerosis complex: a review. Semin. Pediatr. Neurol. 13, 27–36.

Ruppe, V., Dilsiz, P., Reiss, C.S., Carlson, C., Devinsky, O., Zagzag, D., Weiner, H.L., and Talos, D.M. (2014). Developmental brain abnormalities in tuberous sclerosis complex: a comparative tissue analysis of cortical tubers and perituberal cortex. Epilepsia 55, 539–550.

Santini, E., Huynh, T.N., MacAskill, A.F., Carter, A.G., Pierre, P., Ruggero, D., Kaphzan, H., and Klann, E. (2013). Exaggerated translation causes synaptic and behavioural aberrations associated with autism. Nature 493, 411–415.

Sarbassov, D.D., Guertin, D.A., Ali, S.M., and Sabatini, D.M. (2005). Phosphorylation and regulation of Akt/PKB by the rictor-mTOR complex. Science 307, 1098–1101.

Shah, O.J., and Hunter, T. (2006). Turnover of the active fraction of IRS1 involves raptor-mTOR- and S6K1-dependent serine phosphorylation in cell culture models of tuberous sclerosis. Mol. Cell. Biol. 26, 6425–6434.

Shi, Y., Kirwan, P., Smith, J., Robinson, H.P., and Livesey, F.J. (2012). Human cerebral cortex development from pluripotent stem cells to functional excitatory synapses. Nat. Neurosci. 15, 477–486, S1.

Talos, D.M., Kwiatkowski, D.J., Cordero, K., Black, P.M., and Jensen, F.E. (2008). Cell-specific alterations of glutamate receptor expression in tuberous sclerosis complex cortical tubers. Ann. Neurol. 63, 454–465.

Talos, D.M., Sun, H., Kosaras, B., Joseph, A., Folkerth, R.D., Poduri, A., Madsen, J.R., Black, P.M., and Jensen, F.E. (2012). Altered inhibition in tuberous sclerosis and type IIb cortical dysplasia. Ann. Neurol. 71, 539–551.

Tang, G., Gudsnuk, K., Kuo, S.H., Cotrina, M.L., Rosoklija, G., Sosunov, A., Sonders, M.S., Kanter, E., Castagna, C., Yamamoto, A., et al. (2014). Loss of mTOR-dependent macroautophagy causes autistic-like synaptic pruning deficits. Neuron 83, 1131–1143.

Tavazoie, S.F., Alvarez, V.A., Ridenour, D.A., Kwiatkowski, D.J., and Sabatini, B.L. (2005). Regulation of neuronal morphology and function by the tumor suppressors Tsc1 and Tsc2. Nat. Neurosci. 8, 1727–1734.

Tee, A.R., Manning, B.D., Roux, P.P., Cantley, L.C., and Blenis, J. (2003). Tuberous sclerosis complex gene products, Tuberin and Hamartin, control mTOR signaling by acting as a GTPase-activating protein complex toward Rheb. Curr. Biol. 13, 1259–1268.

Voineagu, I., Wang, X., Johnston, P., Lowe, J.K., Tian, Y., Horvath, S., Mill, J., Cantor, R.M., Blencowe, B.J., and Geschwind, D.H. (2011). Transcriptomic analysis of autistic brain reveals convergent molecular pathology. Nature 474, 380–384.

Yoon, K.J., Nguyen, H.N., Ursini, G., Zhang, F., Kim, N.S., Wen, Z., Makri, G., Nauen, D., Shin, J.H., Park, Y., et al. (2014). Modeling a genetic risk for schizophrenia in iPSCs and mice reveals neural stem cell deficits associated with adherens junctions and polarity. Cell Stem Cell 15, 79–91.